The Turbulent Wake of a Monopile Foundation

C.Rogan*, J.Miles**, D.Simmonds**, G.Iglesias**

School of Marine Science and Engineering, Plymouth University, Plymouth, PL4 8AA, UK

Abstract

An experimental programme is presented, examining the turbulent wake of a monopile foundation in a current. Velocity was recorded across an extensive domain downstream of a model monopile in a 0.5 m deep basin, using an acoustic Doppler velocimeter array. The distribution of turbulent kinetic energy (TKE) is examined across the entire domain. Tests were undertaken using several combinations of pile diameter ($D = 0.1$ and 0.2 m) and mean flow velocity ($\bar{u_0} = 0.08$ to 0.24 m/s), representing typical prototype conditions at a scale of 1:50. It is shown that turbulence can be predicted using the distance downstream (x) and off axis (y), the pile diameter, and the mean flow velocity. Two new parameters are introduced to simplify assessment of proposed structures. Relative Excess Turbulence (RET) is the extra turbulence generated by the pile, normalised by the ambient turbulence. Turbulence Recovery Lengthscale (TRL) is the distance downstream (normalised by D) required for RET to fall below a given threshold. Results show that RET decays exponentially with distance downstream. Across the wake, RET fitted a Gaussian function with peak values at the wake centreline. TRL is estimated at 40 for an RET threshold of 1.0 and 400 for an RET threshold of 0.1.

Keywords: monopile, turbulence, windfarm, monopile array, windfarm environmental impact, current

*Principle corresponding author. Tel.: +44 7749 545477

**Corresponding author. Tel.: +44 1752 584737; Fax: +44 1752 586101

Email addresses: `charlie.rogan@plymouth.ac.uk` (C.Rogan), `j.r.miles@plymouth.ac.uk` (J.Miles), `d.simmonds@plymouth.ac.uk` (D.Simmonds), `gregorio.iglesias@plymouth.ac.uk` (G.Iglesias)

1. Introduction

Monopile foundations are by far the most common design for offshore wind turbines, comprising 91% of all European installations completed in 2014 (EWEA, 2015). They are well suited to shallow and transitional water depths, due to their simplicity of installation. At existing installations, piles are typically around 5 m in diameter. The UK is currently the world leader in terms of offshore wind installed capacity, with further growth in the sector forming a key component of the government's renewables 2020 strategy (DECC, 2013, Esteban et al., 2011).

As installations move into deeper water and turbine diameters increase, the greater horizontal loads and bending moments will necessitate the use of ever larger piles (Byrne and Houlsby, 2003). There are plans for turbines of 6 MW capacity, in as much as 30 m of water depth. Such installations will require monopiles of up to 7.5 m diameter (Achmus et al., 2008). With a greater number of ever larger monopiles anticipated in the coming years, it is important that we understand their impact.

The flow structure close to the base of a monopile has already been extensively studied (Dargahi, 1989, García-Hermosa et al., 2014, Sumer et al., 1997, Unger and Hager, 2006). Three distinct flow structures can be identified close to the base of the pile. A horseshoe vortex forms at the upstream face, contraction of streamlines occurs as the flow accelerates around the sides of the pile, and lee wake vortices are formed immediately downstream of the pile.

These flow structures lead to enhanced bed scour and the formation of a scour hole around the pile. This is of great concern to the structural integrity of the foundation. Much work has been done to quantify the depth of the scour hole (Roulund et al., 2005, Sumer et al., 2001, Whitehouse et al., 2011), and its rate of development (McGovern et al., 2014).

In addition to the flow structures described above, the monopile's presence will cause increased turbulence in the flow downstream. Elevated turbulence enhances the carrying capacity of the flow, leading to increased sediment transport (Butt et al., 2004, Gyr and Hoyer, 2006). This increases the distance that scoured sediments can be transported downstream of the pile.

The environmental impacts of suspended sediments are numerous. Increased turbidity can affect the productivity of plankton (Kocum et al., 2002), as well as influencing the behaviour of predatory fish (Abrahams and Kattenfeld, 1997) and marine mammals (Weiffen et al., 2006). These are related to economic concerns, as any changes could impact on fisheries. Sediment transport regimes also govern sedimentation processes downstream (Yin et al., 2014).

Techniques exist for estimating the turbidity downstream of existing monopiles, by analysing satellite images (Gerace et al., 2013). Turbid wakes have been observed transporting sediment for hundreds of metres downstream of monopiles (Vanhellemont and Ruddick, 2014).

Ideally, numerical modelling would be used to predict the likely impact of a proposed wind farm on sediment transport during the planning phase. However, the flow structures governing the increased turbulence are typically on the same scale as the monopile. These cannot be resolved by existing sediment transport models, which typically have cell sizes on the order of hundreds of meters in order to cope with the large regions of interest (Magar et al., 2013).

This paper presents the results of a series of laboratory experiments, performed at a scale of 1:50, examining the wake structure downstream of a monopile foundation. In particular, the influence on turbulence of flow velocity, pile diameter and location relative to the pile were measured. Two new parameters are introduced to simplify turbulence assessment of planned monopile structures in terms the relative position and flow velocity.

Empirical relationships are presented predicting the turbulent characteristics of the wake. These have been validated to show that turbulence in the wake of a monopile can be described by a small number of parameters. These parameterisations will allow the monopile's influence on turbulence to be implemented in regional sediment transport models.

2. Materials and Methods

2.1. Experimental Design

The experimental programme was carried out in the Coastal basin at Plymouth University. The basin measures 10 m long by 7.2 m wide, with a water depth of 0.5 m. The pile was fixed to the floor of the basin, centred 4.5 m from the downstream tank wall and 3.5 m from the side (Figure 1). The floor of the tank is fibre reinforced plastic, with a roughness lengthscale of < 0.0001 m.

Prototype values of water depth, pile diameter and flow velocity were chosen based on typical values at existing wind farm sites. Matutano et al. (2013)

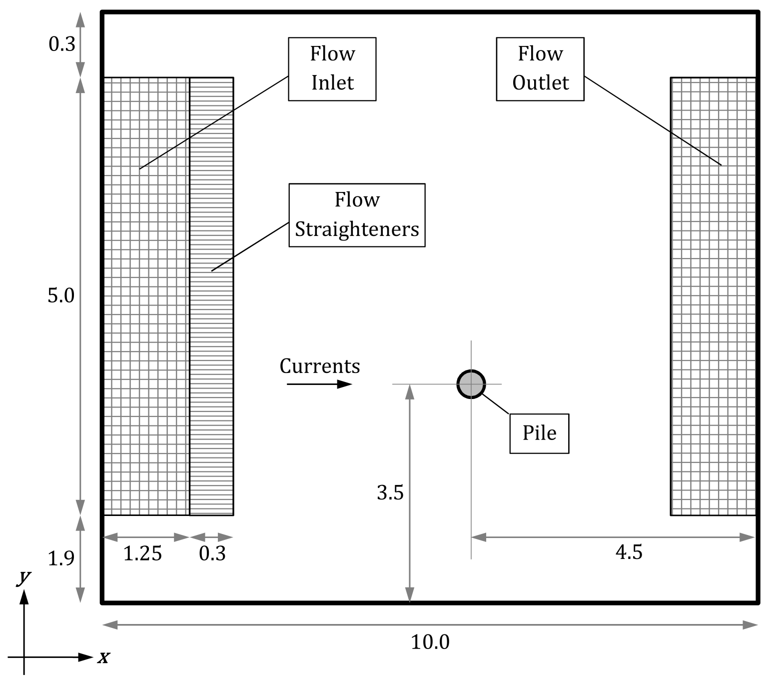

Figure 1: Plan view of the Coastal basin. Not to scale. All dimensions in metres.

provide information from several existing wind farms. Average monopile diameter is just below 5 m, with the largest quoted at 6 m. Pile diameters are expected to increase in the future as development moves into deeper water. Peak current velocities range between 0.6 and 2.0 m/s, although the higher values in this range correspond to particularly shallow sites. The experimental programme was designed to examine turbulence in the free stream flow, and so an intermediate depth prototype was considered more appropriate. This was confirmed by examination of proposed sites in the channel region, using the ANEMOC offshore windfarm database (Benoit et al., 2008).

Prototype values were converted to model scale by applying Froude similitude at a scale of 1:50 to derive appropriate scale factors (λ). Measurements were made at four model velocities ($\bar{u_0} = 0.08$, 0.14, 0.18 and 0.24 m/s), and two model pile diameters ($D = 0.1$ and 0.2 m), in water depth d of 0.5 m (Table 1). Froude similitude is achieved between the model and prototype, with Froude numbers ranging between 8×10^{-2} and 2×10^{-1}.

Table 1: Prototype vs Model parameters

Parameter	λ	Prototype	Model
d	50	25 m	0.5 m
D	50	5-10 m	0.1-0.2 m
$\bar{u_0}$	$\sqrt{50}$	0.6-1.6 m/s	0.08-0.24 m/s
Re	-	2×10^6 to 2×10^7	8×10^3 to 5×10^4

Measured water temperatures were around 20 °C throughout the experimental program, with a corresponding kinematic viscosity of approximately 10^{-6} m^2/s. For the current experimental program, model Reynolds numbers range from 8×10^3 to 5×10^4; flow is fully turbulent.

To allow comparison of results with different prototype scales, x and y positions were normalised by the pile diameter to yield x^* and y^*:

$$x^* = \frac{x}{D} \qquad (1) \qquad\qquad y^* = \frac{y}{D} \qquad (2)$$

2.2. Data

Three components of velocity were measured using a Nortek Vectrino profiler Acoustic Doppler Velocimeter (ADV), referred to here as 'ADV1'. ADVs are very suitable for experimental measurements of this kind and are widely used, (Graf and Istiarto, 2002, Qi et al., 2012). Nikora and Goring (1998) provide a summary of their operation.

Detailed velocity measurements were made downstream of the model pile under steady flow conditions, with the goal of parameterising the wake structure. Velocity time series data were recorded using ADV1 positioned along transverse and longitudinal wake profiles (Figure 2). At each location, 500 seconds of velocity time series data were recorded at a sample frequency of 64 Hz, for each flow condition. The instrument was positioned vertically to record point velocity within the free stream, 35 cm from the tank floor.

The longitudinal profile extended 2.7 m downstream of the pile centre, with nine measurement positions spaced logarithmically along its length. Table 2 summarises the eight transverse profiles, aligned perpendicular to the mean flow. Values of x and D were chosen so that the eight profiles converged to four in the x^* domain. Each profile extended 50 cm either side of the wake centreline.

Table 2: Summary of transverse profiles

D (m)	x (m)	x^* -	$\bar{u_0}$ (m/s)
0.1	0.25	2.5	0.08-0.18
0.1	0.50	5.0	
0.1	0.75	7.5	
0.1	1.00	10.0	
0.2	0.50	2.5	0.08-0.24
0.2	1.00	5.0	
0.2	1.50	7.5	
0.2	2.00	10.0	

Velocity time series data from ADV1 was used to calculate Turbulent Kinetic Energy per unit volume (TKE), using equation 3.

$$TKE = \frac{1}{2}\rho(\bar{u'^2} + \bar{v'^2} + \bar{w'^2}) \tag{3}$$

Where u, v and w are the components of velocity in the x, y and z directions, respectively, and the apostrophe indicates the fluctuating component. ρ is the density of water. For these experiments, x is defined as the mean flow direction, y is the other horizontal dimension perpendicular to this, and z is the vertical direction.

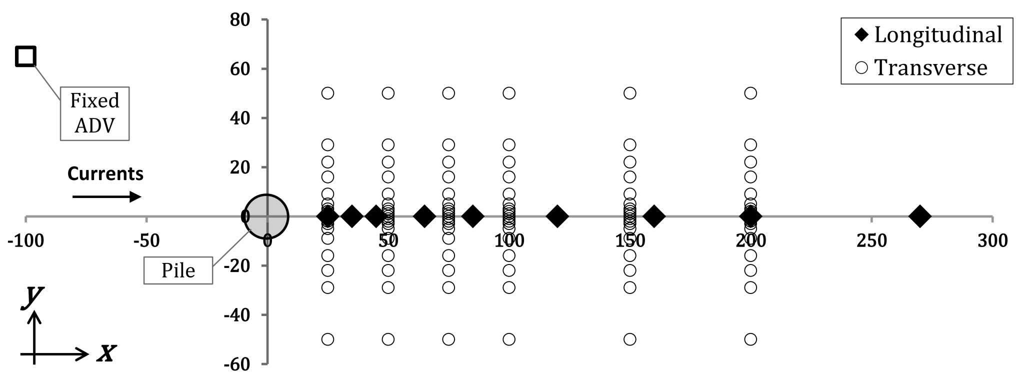

Figure 2: Experimental setup: plan view showing longitudinal and transverse measurement profiles. All dimensions in cm.

A point measurement ADV (Nortek Vectrino+) was used to measure the undisturbed mean flow velocity upstream of the pile ($\bar{u_0}$). This instrument, referred to as 'ADV2', was positioned 100 cm upstream of the pile centre and +65 cm off axis. The two instruments had the same sample frequency, and were electronically synchronised to record over the same time period. Both instruments were positioned vertically so as to measure within the free stream, 35 cm from the tank floor.

2.3. Control Measurements

A series of control measurements were also made with the pile removed from the tank. These covered the same range of pump settings as used in the wake measurements. Control TKE values (TKE_0) were calculated from the velocity time series data according to equation 3.

2.4. Flow Conditioning

Flow entering the tank passed through a flow straightener structure to minimise pump turbulence. Design of this structure was informed by the findings of Markus et al. (2015). Flow is impounded near the inlet, before passing through a bank of honeycomb blocks to enter the basin. Each block measures 0.5 m tall by 0.3 m thick by 1.25 m wide, with a bank of four blocks extending across 5.0 m of the inlet grills. The blocks are made from polycarbonate with a cell size of 12 mm diameter. Whilst Markus et al. used tubes aligned both parallel and perpendicular to the main flow direction, all of the cells in the current work were aligned parallel to the flow. Visual examination of the flow with fine seeding particles confirmed that turbulence is not significant once the flow has passed through the honeycomb.

2.5. Data Pre-Processing

In order to reduce the potential problems of instrument noise and ensure that genuine turbulent fluctuations were identified, raw measurements were subjected to rigorous processing to ensure high quality data. Data were assessed manually to check for low correlation, low signal to noise ratio, reflections from the bed, or phase wrapping - all indications of poor measurement accuracy. Acceptable data were then filtered using a 3D phase space algorithm to remove noise. This technique was originally proposed by Goring and Nikora (2002), and modified by Wahl (2003). A concise description of the algorithm can be found in Mori et al. (2007).

2.6. New Parameters

In assessing the environmental impact of a proposed monopile foundation, a fundamental consideration is the increase in turbulence relative to the ambient level in the undisturbed flow (TKE_0). To this end, a new parameter is introduced to express the increased turbulence in the pile wake - the Relative Excess Turbulence (RET):

$$RET = \frac{TKE - TKE_0}{TKE_0} \tag{4}$$

Another useful parameter for impact assessment is the spatial extent of the pile's region of influence. A second new parameter is introduced to simplify comparisons between proposed installations. The Turbulence Recovery Lengthscale (TRL) is defined as the normalised distance required downstream, along the wake centreline, for turbulence to recover. Recovery can be considered to have taken place when RET falls below a threshold (Δ).

$$TRL = x^* \tag{5}$$

when

$$y^* = 0 \qquad \text{and} \qquad RET = \Delta$$

3. Results

Data from the experimental programme were analysed, with the aim of quantifying a surface that defines RET in the domain downstream of a pile in terms of x^* and y^*.

3.1. Control Measurements

The data from the control measurements is presented in Table 3. These values are the mean of three measurements made using ADV1 at each of four pump settings. As expected, pump power correlates with both $\bar{u_0}$ and TKE_0. Following the quadratic relationship between velocity and kinetic energy, TKE_0 was normalised by $\rho\bar{u_0}^2$. Values of $TKE_0/\rho\bar{u_0}^2$ show close agreement across the range of flow conditions tested, supporting this method of normalising TKE.

Table 3: Summary of control data

Pump Power (%)	$\bar{u_0}$ (m/s)	TKE_0 (kg m^{-1} s^{-2})	$TKE_0/\rho\bar{u_0}^2$ -
20	0.0963	0.1289	0.0139
32	0.1531	0.3694	0.0158
40	0.1886	0.5459	0.0153
50	0.2357	0.8471	0.0153

3.2. Longitudinal Characteristics

Figure 3a shows measured TKE values along the centreline of the wake downstream of the 10 cm pile, at each of the three current velocities tested. Turbulence decays exponentially with distance downstream of the pile in all three datasets. As expected, higher mean flow velocity correlates with higher values of TKE. These trends were also observed downstream of the 20 cm pile. Figure 3b shows trends with similar gradients, this time for four different velocities tested. For a given value of x at or beyond 0.5 m, TKE values associated with the larger pile are greater by a factor of approximately two.

TKE and x can be normalised by $\rho\bar{u_0}^2$ and D respectively. When this was applied, data for both pile diameters and all four mean flow velocities collapsed towards a common relationship, as shown in Figure 4. Data nor-

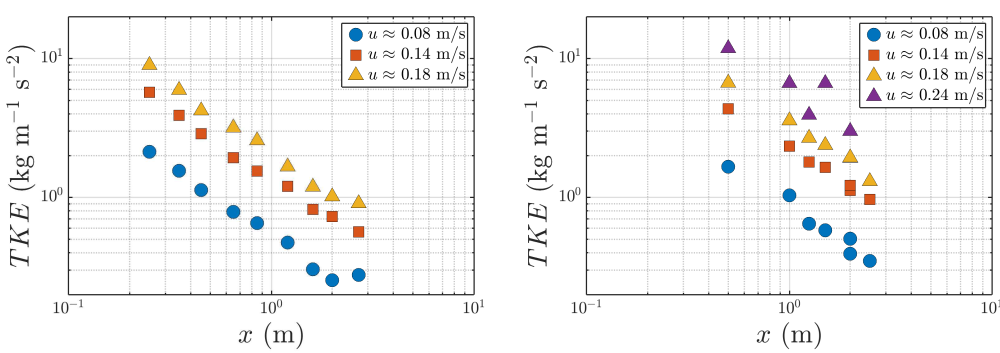

(a) 10 cm diameter pile.

(b) 20 cm diameter pile.

Figure 3: Centreline TKE Profiles

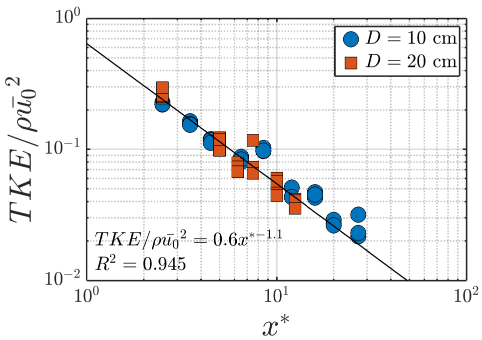

Figure 4: Normalised TKE: longitudinal profiles. $\bar{u_0} = 0.08$ to 0.18 m/s

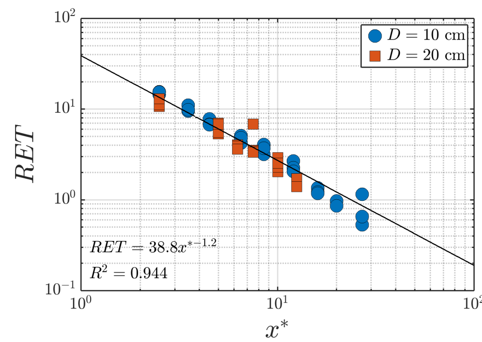

Figure 5: RET: longitudinal profiles. $\bar{u_0} = 0.08$ to 0.24 m/s

malised in this way were analysed using linear regression to yield equation 6, which fits the data with an R^2 of 0.945. The high R^2 value indicates that the equation is very representative of the process. This shows that turbulence characteristics downstream of the pile centreline can be estimated using only $\bar{u_0}$ and D, parameters that will be known at an early design stage.

$$\frac{TKE}{\rho\bar{u_0}^2} = 0.6x^{*-1.1} \tag{6}$$

The wake TKE data from ADV1 were combined with undisturbed velocity data from ADV2, to calculate RET (equation 4). When this was applied, data for both pile diameters and all four mean flow velocities collapsed to a single relationship (Figure 5). Equation 7 fits the measured data with an R^2 value of 0.944. Both equation 6 and equation 7 can be applied with confidence over the experimental range of $2.5 \leq x^* \leq 27$.

$$RET = 38.8x^{*-1.2} \tag{7}$$

3.3. Transverse Characteristics

Figure 6 shows a typical transverse profile of normalised TKE. Normalised TKE was greatest along the wake's centreline, and rapidly dropped to a constant background value on either side. Transverse TKE cross sections collapsed when normalised by mean $\rho\bar{u_0}^2$ and D, as was the case with the longitudinal profiles.

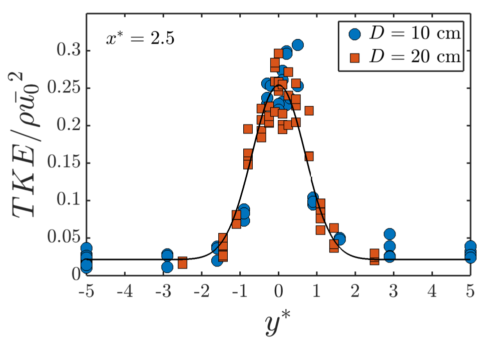

Figure 6: Normalised TKE cross section, 2.5 D downstream. Data for different velocities and pile diameters collapsed to a common relationship.

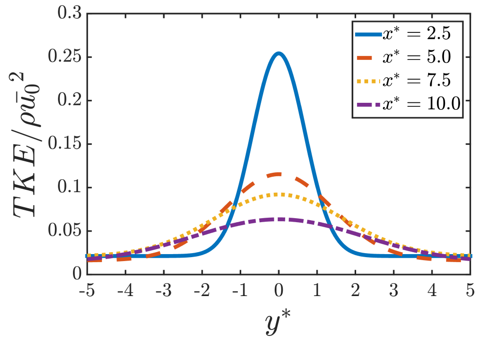

Figure 7: Transverse profiles fitted to normalised TKE data at four different values of x^*. Cross sections become lower and wider with x^*.

The distribution of TKE in the cross sections was found to fit a function of the form:

$$\frac{TKE}{\rho\bar{u_0}^2} = \alpha_1 e^{-\alpha_2 y^{*2}} + \alpha_3 \tag{8}$$

Where α_1, α_2 and α_3 are regression constants. Non-linear regression was used to determine the values of these constants for each of the four x^* profiles (Table 4).

Table 4: Regression constants for normalised TKE cross sections.

x^*	α_1	α_2	α_3	R^2
2.5	0.2330	1.0512	0.0212	0.9387
5.0	0.0992	0.2555	0.0162	0.7892
7.5	0.0711	0.1748	0.0209	0.5396
10.0	0.0497	0.1015	0.0138	0.5826
Mean	-	-	0.0180	0.7125

For a given cross section, the peak value of TKE is governed by the constant α_1. Given the distance downstream and the pile diameter, the value of α_1 might be estimated using equation 6. Likewise, the width of the wake is governed by the constant α_2. Both constants tend towards zero as x^* increases and the wake profile becomes lower, wider and flatter (Figure 7).

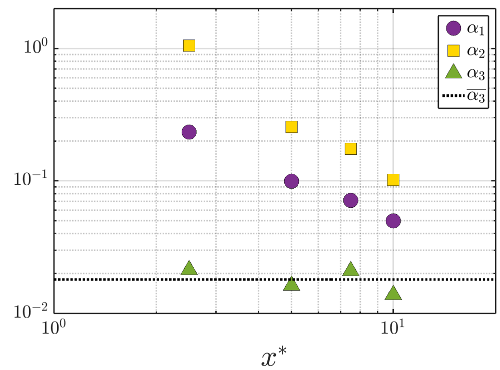

Figure 8: Regression constants α_1, α_2 and α_3 for normalised TKE cross sections.

Figure 8 plots the values of α_1, α_2 and α_3 against x^*, confirming the trend identified in Table 4. Although α_1 and α_2 are constant for a given cross section, these observations show that when considering the wake as a whole they are functions of x^*.

The constant α_3 defines the ambient level to which turbulence decays outside the wake. The fitted values were similar for all four cross sections. Furthermore, the range of α_3 encompasses the control range of $TKE_0/\rho\bar{u_0}^2$ presented in Table 3, with similar mean values.

Figure 9 plots RET against y^*, for each of the four values of x^* tested. Each plot represents two different pile diameters and four different flow velocities. As with the longitudinal profiles, the data collapse very well when normalised in this way. Peak RET occurs along the centreline. The shape of the wake becomes lower, flatter and wider as x^* increases.

Table 5: Regression constants for RET cross sections.

x^*	β_1	β_2	R^2
2.5	14.1747	0.9429	0.9309
5.0	6.7866	0.3028	0.8332
7.5	5.1888	0.1657	0.5292
10.0	2.8917	0.0928	0.4760
$Mean$	-	-	0.6923

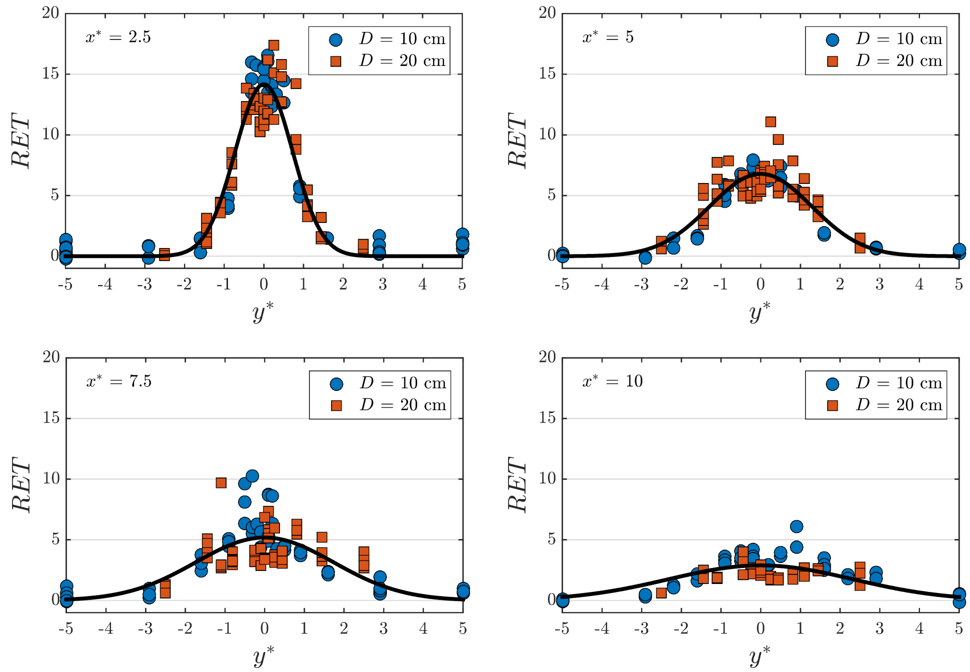

Figure 9: RET - transverse cross sections at different values of x^*. Black lines indicate equation 9 fitted to the measured data. Profiles become lower, flatter and wider as x^* increases.

Average RET values recover to approximately zero at the boundaries of the wake. This allows equation 8 to be simplified to give equation 9:

$$RET = \beta_1 e^{-\beta_2 y^{*2}} \tag{9}$$

Table 5 summarises the fitting of experimental data to this relationship. As with Table 4, the values of the constants tend towards zero as x^* increases. The general trend in both tables is for R^2 to reduce with increasing values of x^*. This might be attributed to the increasing influence of measurement error as the turbulence signal decreases. Figure 9 indicates that equation 9 predicts the mean RET values at the crest of each profile.

3.4. Empirical model

Following the observations made in sections 3.2 and 3.3, a unifying relationship was sought to describe the distribution of turbulence over the entire domain. The validity of such a relationship follows from dimensional analysis of the parameters. As the peak RET in a given cross section occurs along the centreline, β_1 can be expressed by a term of the same form as equation 7; $\beta_1 = \gamma_1 x^{*-\gamma_2}$, where γ_1 and γ_2 are constants. Table 5 suggests an inverse relationship between x^* and β_2, and so the term γ_3/x^* is substituted for β_2, where γ_3 is a constant. RET can now be expressed in terms of both x^* and y^*:

$$RET = \gamma_1 x^{*-\gamma_2} e^{-\frac{\gamma_3 y^{*2}}{x^*}} \tag{10}$$

Using non-linear regression, equation 10 was fit to the measured data to yield the constants γ_1, γ_2 and γ_3. Equation 10 is valid with these constants for the range of experimental values, $2.5 \leq x^* \leq 27$ and $-5 \leq y^* \leq 5$.

$$\gamma_1 = 33.949$$
$$\gamma_2 = 0.9761$$
$$\gamma_3 = 1.9967$$

Along the centreline of the wake, γ_1 and γ_2 are analogous and similar in magnitude to the fitted constants in equation 7, which gives confidence in the result.

Figure 10 plots the measured data over the entire domain, against a surface defined by the empirical relationship. Measured RET agrees closely with calculated values. The function successfully explains both the exponential decay of RET along the wake centreline and the spreading of the wake with distance downstream.

Figure 11 plots the measured values of RET against those predicted using equation 10 and the fitted values of γ_1, γ_2 and γ_3. Predicted values were found to fit measured data with an R^2 of 0.874. 23% of predicted values are within ±10% of the measured data, with 70% falling within ±50%.

3.5. Outputs

Equation 10 allows the calculation of TRL along the wake centreline. By setting y^* equal to zero and RET equal to Δ, γ_3 is eliminated and the equation simplifies:

$$\gamma_1 x^{*-\gamma_2} = \Delta \tag{11}$$

$$x^* = e^{\frac{ln \frac{\gamma_1}{\Delta}}{\gamma_2}} = TRL \tag{12}$$

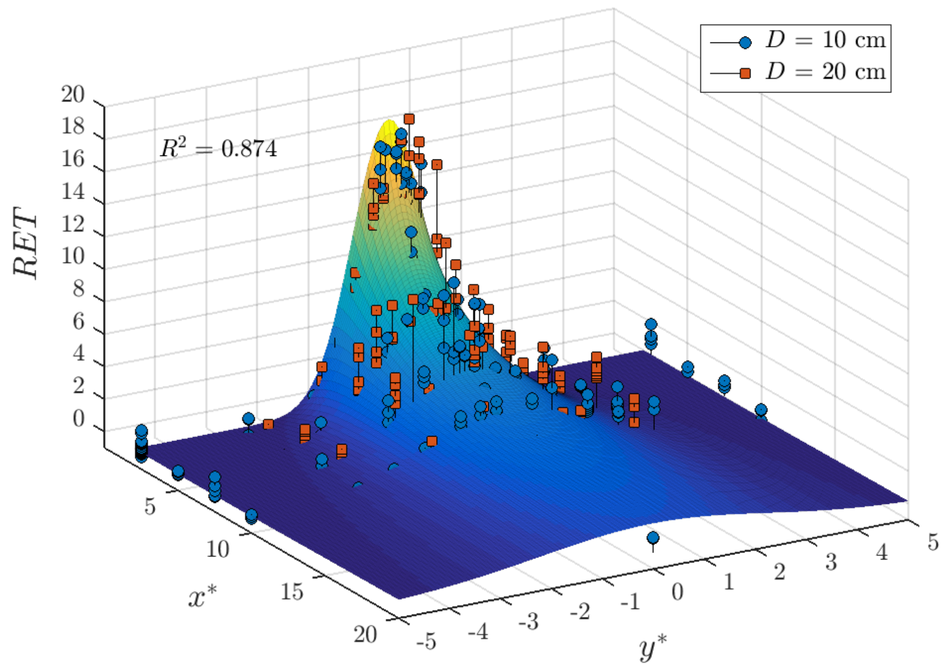

Figure 10: Distribution of Residual Excess Turbulence (RET), against normalised distance downstream (x^*) and off axis (y^*) from the pile centre. Measured values against a surface defined by equation 10.

The value of the threshold Δ is arbitrary in this definition, and different values may be specified according to the purpose of the analysis. Two examples serve to illustrate this point:

Given a receptor or process that is insensitive to variations in turbulence, Δ might be set equal to 1.0. This implies TKE is twice that of the ambient conditions, and might signify that turbulence has returned to its original order of magnitude. Inputting these values into equation 12 yields a value of 37.01 for TRL, or approximately 40. Given a typical prototype diameter of 5 m, this corresponds to a distance of 200 m. From an engineering perspective, 200 m is less than typical turbine spacing in existing and planned offshore windfarms; RET will decay below a value of 1.0 before reaching a neighbouring monopile.

If instead the process of interest is highly sensitive to changes in turbu-

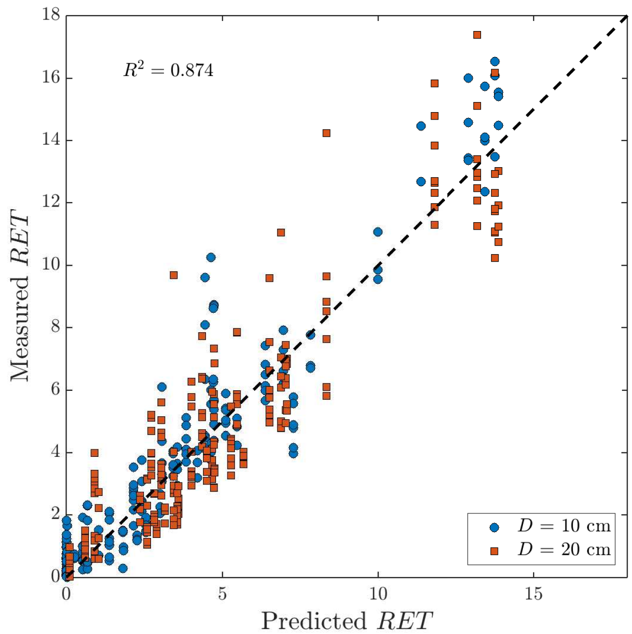

Figure 11: RET downstream of the pile. Measured values vs values predicted using equation 10.

lence, a value of 0.1 might be specified for the threshold Δ. This implies that TKE has decayed to only 10% above the ambient conditions - a much tighter specification than above. Using this new threshold TRL is calculated at 391.6, or approximately 400. This corresponds to 2,000 m downstream for a typical 5 m diameter prototype, which is greater than typical pile spacing; RET will exceed 0.1 when the wake reaches the next pile downstream.

4. Discussion

Model velocities covered the range from 0.08 to 0.24 m/s. These model values represent prototype current velocities of 0.57 to 1.70 m/s, which are typical of peak velocities measured at existing wind farms (Matutano et al., 2013). The data may even be applicable to some less energetic tidal energy sites.

Two pile diameters were tested during the experimental programme. The 0.1 m model pile scales to a typical 5 m diameter prototype in a transitional water depth of 25 m. At the same scale, the 0.2 m pile represents a 10 m diameter prototype. This is significantly larger than the largest wind turbine monopiles currently being proposed, but may represent other types of offshore structure. In spite of this disparity in scale, RET values collapsed successfully (Figure 5, Figure 9, Figure 11). This suggests that the relationships identified hold true for the range of pile diameters scaled to represent existing and proposed offshore wind farms.

In general, the proposed equations were found to represent the data well. One group of RET values were found to lie above the main cluster of data in the cross section at $x^* = 7.5$ (Figure 9). Closer examination did not reveal any underlying cause for this group of points. Despite these anomalous data, the range of RET values at the centre of the cross section is approximately 8, which is similar to the range of RET values shown in the cross sections at $x^* = 2.5$ and $x^* = 5$.

The findings indicate that turbulence affects a substantial region downstream of the pile, showing that turbulence is a much larger scale problem than scour. Changes to the turbulent characteristics of the flow may be significant for mixing, and could affect primary productivity and marine biodiversity in the region of the pile (Kocum et al., 2002).

This is in good agreement with the findings of Vanhellemont and Ruddick (2014), who reported turbid plumes 30 to 150 m wide, extending for several kilometres downstream of wind farms. Translating RET values into quantities of suspended particulate matter would require data on the characteristics of the suspended material and the ambient conditions at a specific site, as proposed by Rivier et al. (2014). However, heightened TKE at this distance from the pile will enhance the carrying capacity of the flow, and contribute to the persistence of the observed plumes.

Prototype pile spacing within existing and planned wind farms is typically 500 to 1,000 m, with pile diameters of around 5 m. Given these dimensions, the TRL values estimated in section 3.5 imply that the RET reaching a monopile from its upstream neighbour will be somewhere between 1.0 and 0.1. This is small compared to the estimated RET of 33.9 at $x^* = 1.0$ downstream of an individual pile (equation 10). These observations suggest that monopile foundations will behave as individuals with respect to turbulence in the pile wake, and group effects are expected to be small.

5. Conclusion

A detailed experimental programme was carried out in a laboratory to assess the levels of turbulence in the wake of a monopile foundation. TKE measurements were made up to 27 diameters downstream of the pile. Turbulence along the wake centreline was found to decay exponentially with distance downstream.

In this work, two new parameters have been introduced for characterising the turbulence downstream of a monopile foundation: the Relative Excess Turbulence (RET) and the Turbulence Recovery Lengthscale (TRL). These parameters will be useful for assessing the likely impact of monopile foundations on local flow conditions. Experimental data were used to infer TRL values of 40 pile diameters for an RET threshold of 1.0, or 400 pile diameters for an RET threshold of 0.1.

Profiles of turbulence across the wake fitted a Gaussian function. The lateral extent of the pile's impact increased with distance downstream of the pile. Measurements of TKE outside the wake were similar to ambient values.

6. Acknowledgements

This work was carried out as part of the OFELIA project (Offshore Foundations EnvironmentaL Impact Assessment). This is a collaboration between the universities of Plymouth, Le Havre and Caen, and the authors would like to thank all project partners for their support and constructive comments. The project was selected under the European cross-border cooperation programme INTERREG IV A France (Channel) - England, co-funded by the ERDF (European Regional Development Fund).

References

Abrahams, M. and Kattenfeld, M. (1997), 'The role of turbidity as a constraint on predatory-prey interactions in aquatic environments.', *Behavioural Ecology and Sociobiology* **40**, 169 – 174.

Achmus, M., Abdel-Rahman, K. and Kuo, Y.-S. (2008), Design of Monopile Foundations for Offshore Wind Energy Converters, *in* '11th Baltic Sea Geotechnical Conference', Gdansk.

Benoit, M., Lafon, F. and Goasguen, G. (2008), 'Constitution et exploitation d'une base de données d'états de mer le long des côtes françaises par simulation numérique sur 23 ans', *European Journal of Environmental and Civil Engineering* **12**(February 2015), 35–50.

Butt, T., Russell, P., Puleo, J., Miles, J. and Masselink, G. (2004), 'The influence of bore turbulence on sediment transport in the swash and inner surf zones', *Continental Shelf Research* **24**, 757–771.

Byrne, B. W. and Houlsby, G. T. (2003), 'Foundations for offshore wind turbines', *Philosophical Transactions of The Royal Society* **361**, 2909–2930.

Dargahi, B. (1989), 'The turbulent flow field around a circular cylinder', *Experiments in Fluids* **12**, 1–12.

DECC (2013), UK Renewable Energy Roadmap, Technical Report November, Department of Energy and Climate Change.

Esteban, M. D., Diez, J. J., López, J. S. and Negro, V. (2011), 'Why offshore wind energy?', *Renewable Energy* **36**(2), 444–450.

EWEA (2015), The European offshore wind industry - key trends and statistics 2014, Technical Report January, European Wind Energy Association.

García-Hermosa, I., Brossard, J., Cohen, Z., Perret, G., Pinon, G., Abcha, N., Bennis, A. C., Ezersky, A., Mouazé, D., Rivier, A., Iglesias, G., Miles, J., Rogan, C., Simmonds, D., Gross, M. and Magar, V. (2014), Experimental characterisation of wave induced flow fields due to an offshore wind farm mast, *in* 'Proceedings of the 1st International Conference on Renewable Energies Offshore', Lisbon.

Gerace, A. D., Schott, J. R. and Nevins, R. (2013), 'Increased potential to monitor water quality in the near-shore environment with Landsat's next-generation satellite', *Journal of Applied Remote Sensing* **7**, 073558–1 – 073558–18.

Goring, D. G. and Nikora, V. I. (2002), 'Despiking acoustic doppler velocimeter data', *Journal of Hydraulic Engineering* **128**(1), 117–126.

Graf, W. H. and Istiarto, I. (2002), 'Flow pattern in the scour hole around a cylinder Écoulement dans une fosse autour d'un cylindre', *Hydraulic Research* **40**(1), 13–20.

Gyr, A. and Hoyer, K. (2006), *Sediment Transport*, Springer.

Kocum, E., Underwood, G. J. C. and Nedwell, D. B. (2002), 'Simultaneous measurement of phytoplanktonic primary production, nutrient and light availability along a turbid, eutrophic UK east coast estuary (the Colne Estuary)', *Marine Ecology Progress Series* **231**, 1–12.

Magar, V., Abcha, N., Bennis, A., Brossard, J., Conley, D., Ellis, E., Ezersky, A., Greaves, D., Gross, M. S., Iglesias, G., Littlewood, K., Miles, J., Mouazé, D., Perret, G., Pinon, G. and Simmonds, D. J. (2013), Laboratory-Scale Environmental Impact Assessment of a Monopile Foundation under Different Wave Conditions, *in* 'EWEA Offshore 2013', pp. 1–9.

Markus, D., Jakobsen, M., Bletzinger, K.-U. and Frigaard, P. (2015), 'Damping of unwanted turbulence in wave-current experiments', *Coastal Engineering* **96**, 38–48.

Matutano, C., Negro, V., López-Gutiérrez, J.-S., Esteban, M. D. and del Campo, J. M. (2013), 'Dimensionless wave height parameter for preliminary design of scour protection in offshore wind farms', *Journal of Coastal Research* **29**(65), 1633–1638.

McGovern, D. J., Ilic, S., Folkard, A. M., McLelland, S. J. and Murphy, B. J. (2014), 'Time development of scour around a cylinder in simulated tidal currents', *Journal of Hydraulic Engineering* **140**(6).

Mori, N., Suzuki, T. and Kakuno, S. (2007), 'Noise of acoustic doppler velocimeter data in bubbly flows', *Journal of engineering mechanics* **133**(1), 122–125.

Nikora, V. and Goring, D. (1998), 'ADV measurements of turbulence: Can we improve their interpretation?', *Journal of Hydraulic Engineering* .

Qi, W., Gao, F., Han, X. and Gong, Q. (2012), Local scour and pore-water pressure around a monopile foundation under combined waves and currents, *in* 'Proceedings of the Twenty-second International Offshore and Polar Engineering Conference', Rhodes, pp. 159–165.

Rivier, A., Bennis, A. C., Pinon, G., Gross, M. and Magar, V. (2014), 'Modelisation numerique regionale de l'impact des eoliennes offshore sur l'hydrodynamique et le transport sedimentaire', *Journées de l'hydrodynamique* **14**.

Roulund, A., Sumer, B. M., Fredsøe, J. and Michelsen, J. (2005), 'Numerical and experimental investigation of flow and scour around a circular pile', *Journal of Fluid Mechanics* **534**, 351–401.

Sumer, B., Christiansen, N. and Fredsøe, J. (1997), 'The horseshoe vortex and vortex shedding around a vertical wall-mounted cylinder exposed to waves', *Journal of Fluid Mechanics* **332**, 41–70.

Sumer, B., Whitehouse, R. J. and Tørum, A. (2001), 'Scour around coastal structures: a summary of recent research', *Coastal Engineering* **44**(2), 153–190.

Unger, J. and Hager, W. H. (2006), 'Down-flow and horseshoe vortex characteristics of sediment embedded bridge piers', *Experiments in Fluids* **42**(1), 1–19.

Vanhellemont, Q. and Ruddick, K. (2014), 'Turbid wakes associated with offshore wind turbines observed with Landsat 8', *Remote Sensing of Environment* **145**, 105–115.

Wahl, T. (2003), 'Discussion of Despiking acoustic doppler velocimeter data by Derek G. Goring and Vladimir I. Nikora', *Journal of Hydraulic Engineering* **128**(1), 484–488.

Weiffen, M., Möller, B., Mauck, B. and Dehnhardt, G. (2006), 'Effect of water turbidity on the visual acuity of harbor seals (*Phoca vitulina)*', *Vision Research* **46**, 1777–1783.

Whitehouse, R. J. S., Harris, J. M., Sutherland, J. and Rees, J. (2011), 'The nature of scour development and scour protection at offshore windfarm foundations.', *Marine pollution bulletin* **62**(1), 73–88.

Yin, Y., Christie, E., Li, M., Moulinec, C. and Emerson, D. (2014), '3d morphological impact modelling of offshore wind farms using les and hpc', *Coastal Engineering Proceedings* **1**(34), sediment–48.